

ϕ -meson production at RHIC energies using the upgraded PHENIX detector

April 29, 2007

Interim Report submitted to the Feinberg Graduate School of the Weizmann
Institute of Science



Deepali Sharma

Supervisor: Prof. Itzhak Tserruya

Department of Particle Physics

Weizmann Institute of Science

Rehovot, Israel

Abstract

This report describes the work I did during the first year of my Ph.D. This period was mainly devoted to the construction of the Hadron Blind Detector(HBD), which now has been installed in the PHENIX experimental set-up. A prototype detector was constructed to test the key parameters and to measure the performance under test beam conditions. I also participated in two physics runs, run05 in 2005 and run06 in 2006. Currently I am analyzing the run5 pp data and working on the initial commissioning tests of the HBD.

Contents

1	Introduction	4
2	Hadron Blind Detector	5
3	Prototype analysis and Results	6
4	Construction of the final HBD for PHENIX	9
4.1	Vessel construction	9
4.2	Assembly and Testing of GEM foils	10
4.3	Readout electronics	11
5	Present status and Future Plans	12
5.1	HBD Commissioning	12
5.2	Plans	13
6	Run 5 pp analysis	13
	References	16

List of Figures

1	PHENIX detector as of Run 06 with prototype HBD installed	4
2	Gem operation modes: Left panel (FB) and Right panel (RB)	6
3	Matching distributions for hadrons in FB(left) and RB(right). The underlying background of random matches is shown by green line.	7
4	Matching distributions for electrons in FB(left) and RB(right). The underlying background is shown by the green line.	7
5	Pulse height distribution for minimum ionizing particles for detector gain 2200 (a) and 6600 (b) respectively. Black represents FB and red represents RB.	8
6	Charge distribution (a) and cluster size distribution (b) for identified electrons and hadrons with the HBD prototype operated in reverse bias mode.	8
7	The left panel shows a 3-d view of the HBD final design and the right panel shows almost completed one half of the HBD vessel with the pre-amps installed on the back side.	9
8	Gain map of one of the triple GEM stacks presently installed in the HBD	11
9	ADC and Noise distributions for the final HBD	12
10	Track matching along the z - and φ - co-ordinates and E/p distribution for sector E0 and momentum bin 0.05 - 0.35 GeV/c, fitted with gaussian function.	14

11	Mean and Sigma of track matching along z - and φ - co-ordinates and E/p-1 distributions as a function of p_T for one EMCAL sector for the east arm	14
12	The left panel shows the full invariant e^+e^- mass spectrum and the right panel shows the zoomed spectra in ϕ and ω mass region.	15

1 Introduction

Electromagnetic probes are one of the most promising signatures in the quest for the QCD phase transition to the *Quark Gluon Plasma*, the deconfined and chirally restored state of matter predicted by lattice QCD numerical calculations [1]. They have a relatively large mean free path and so leave the interaction region without any final state interaction, carrying information about the conditions and properties of the matter at the time of their production and in particular at the early stages of the collision. The physics potential of low-mass dileptons is well demonstrated by the results from dilepton experiments in heavy-ion collisions like DLS, P325, CERES, HELIOS-3, CBELSA/TAPS, NA38/50. The most prominent result is the enhancement of low-mass electron pairs observed by the CERES [2, 3] experiment at the SPS in all heavy-ion collision systems studied. This enhancement was quantitatively reproduced only by invoking the thermal radiation from a high density hadron gas ($\pi^+\pi^- \rightarrow \rho \rightarrow \gamma^* \rightarrow e^+e^-$) with in-medium modification of the ρ that could be linked to chiral symmetry restoration [4, 5].

The study of low-mass electron pairs under the much better conditions offered at RHIC such as higher initial temperature, larger energy density, larger volume and longer lifetime of the system promises to be very interesting. Calculations [6] predict indeed that the enhancement of low-mass electron pairs observed at SPS persists at the collider with at least a comparable strength. PHENIX [7] is the only experiment at the RHIC with the potential to measure low-mass electron pairs. Fig. 1 shows the PHENIX detector configuration as of run06. The mid-rapidity spectrometers have good electron identification capabilities by combining a RICH detector with an Electromagnetic Calorimeter. However, the current measurements of low-mass electron pairs at PHENIX suffer from a very poor S/B ratio. This is due to the strong magnetic field starting at the collision vertex, causing a limited acceptance of the soft tracks coming from γ -conversions and π^0 -Dalitz decays. This results in a huge combinatorial background that increases quadratically with the number of charged tracks N_{ch} , making signal extraction extremely difficult at the high multiplicities of RHIC. The S/B ratio for the latest PHENIX results, in the mass range $m_{e^+e^-} = 0.3 - 0.5 \text{ GeV}/c^2$ varies from 1/100 to 1/500 depending on p_T cut.

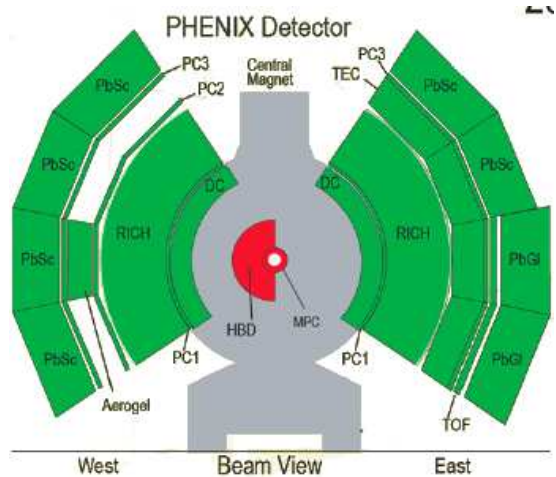


Figure 1: PHENIX detector as of Run 06 with prototype HBD installed

2 Hadron Blind Detector

PHENIX has developed a novel Hadron Blind Detector as an upgrade to overcome this problem. The HBD will recognize and reject the tracks originating from π^0 -Dalitz decays and γ -conversions, by using the fact that the opening angle of electron pairs from these sources is very small compared to pairs of heavier masses. In a field-free region, this angle is preserved and by applying an opening angle cut one can reject more than 90% of the conversions and π^0 -Dalitz decays, while preserving most of the signal. An inner coil, recently installed in the central arms of PHENIX (“+ -” field configuration) counteracts the main field of the outer coils creating an almost field-free region close to the vertex and extending up to ~ 50 - 60 cm in the radial direction. The HBD is located in the field-free region and its size is constrained by this available field-free region.

Conceptual Monte Carlo simulations [8] at the ideal detector level were performed to quantify the potential benefit and define the system specifications of the HBD. A reduction of about two orders of magnitude, in the combinatorial background coming from conversions and π^0 Dalitz decays can be achieved with a detector that provides electron identification with a very high efficiency, at least 90%, double hit recognition at a comparable level and a moderate π -rejection factor of ~ 100 . A somewhat larger acceptance of the HBD ($\delta\phi \leq 135^\circ$ and $|\delta\eta| \leq 0.45$) as compared to the central arms acceptance ($\delta\phi \leq 90^\circ$ and $|\delta\eta| \leq 0.35$), is highly desirable to provide a veto area for the rejection of pairs where only one partner is inside the fiducial acceptance. Finally the detector should have a radiation budget of the order of 1% of radiation length.

A careful evaluation of the relevant options for the key elements (gases, detector configuration and readout chambers) led to the following configuration for the HBD: a windowless Čerenkov detector, operated with pure CF_4 , in a proximity focus configuration, with a CsI photocathode and a triple GEM detector element [9] with pad readout. The use of CF_4 as a radiator and detector gas in a windowless geometry results in a very broad bandwidth (from 6 to 11.5 eV) and a very large figure of merit ($N_0 \sim 840\text{cm}^{-1}$). This corresponds to approximately 36 detected photoelectrons using a 50 cm long radiator, thus ensuring the required level of single electron efficiency and double hit recognition. A CsI photocathode is evaporated on the top surface of the uppermost GEM and the photoelectrons are amplified with a gain of $\sim 5 \times 10^3$ by a triple GEM detector structure with pad readout. In this scheme electrons traversing the radiator produce Čerenkov light forming a “blob” on the pad readout plane. The pads have an hexagonal shape with a size approximately equal to the blob size ($\sim 10\text{cm}^2$) resulting in a low granularity detector.

Fig. 2 shows the configuration of a triple GEM detector in the two different modes in which it can be operated. A bias voltage is applied between the top GEM and the mesh. Depending on the direction of the bias field, charge produced by ionizing particles in the upper gap can either be collected by the GEM (FB = Forward Bias)(right panel), or by the mesh (RB = Reverse Bias)(left panel). In either configuration, photoelectrons produced on the photocathode are collected with good efficiency into the GEM due to the strong electric field near the holes. In the RB mode, only a very small amount of ionization charge produced very near the

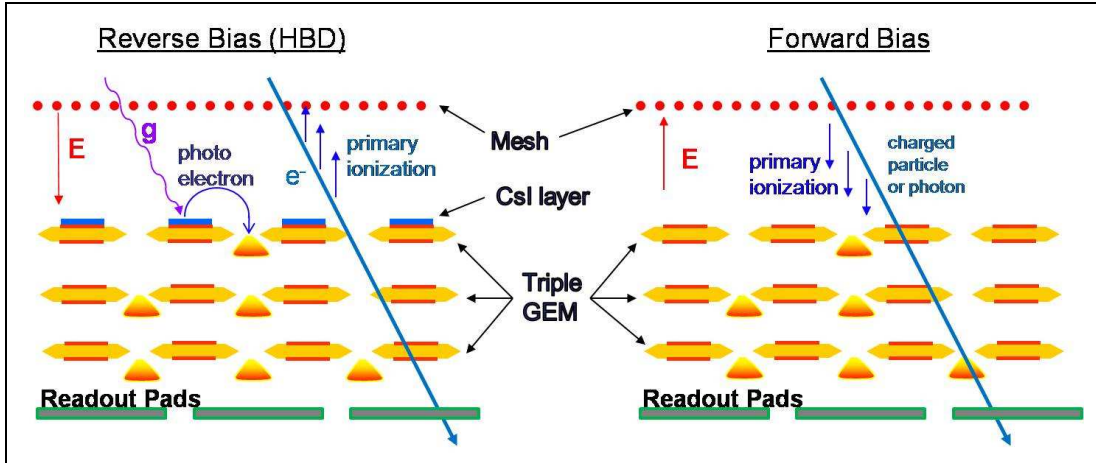


Figure 2: Gem operation modes: Left panel (FB) and Right panel (RB)

photocathode (within $\sim 150\mu\text{m}$) is collected by the GEM. The FB mode is therefore sensitive to hadrons and other charged particles, while the RB mode is essentially sensitive only to the Čerenkov light produced by electrons and hence the term “Hadron Blind”. A comprehensive R&D program was carried out to demonstrate the concept validity including studies in the lab and also a beam test at KEK. The results are published in the two NIM papers [10, 11].

3 Prototype analysis and Results

A full scale prototype similar to the final HBD with one instrumented sector was built and tested under beam conditions (200 GeV pp collisions) in the PHENIX experiment during the early summer of the year 2006 [12]. The magnetic field in the central arms of PHENIX was turned off when HBD data were taken. A few runs were also taken with “+/-” magnetic field configuration. A trigger was set up to enrich the sample of electrons traversing the single instrumented module. The detector showed stable operation with pure CF_4 as the operating gas and worked well in the RHIC environment. A few million events were taken for both configurations of the detector: forward bias and reverse bias.

The prototype had 68 readout channels fully equipped with the same readout chain as foreseen for the final HBD. The signal from the preamps is digitized by a 12 bit flash ADC producing 11 bits of useful information. The best combination for the signal processing was found to be $(S[8] + S[9] + S[10])/3 - S[0]$, where $S[i]$ corresponds to the signal amplitude for i^{th} sample. The analysis was based on the events that had at least one fired pad whose amplitude was greater than 16 ADC counts corresponding to a charge of 1.6 fC. The threshold of 16 ADC counts was decided from the pedestal distributions.

The particle trajectories are reconstructed using the central arm track detectors: Drift Chambers(DC) and Pad Chambers(PC). Valid DC-PC1 tracks are further confirmed by a 3σ matching between the projected and associated hit information at the pad chamber PC3 and EMCal (see Fig. 1). The electron identification is provided

primarily by RICH detector by requiring at least one photomultiplier tube (PMT) hit for the associated track and the energy deposited in the EMCal to be greater than 0.5GeV. For hadrons the selection criteria was opposite i.e. no photomultiplier tube hit in RICH and an associated EMCal cluster energy smaller than 0.5GeV.

The selected hadrons and electrons were matched to HBD hits by a straight line projection onto the HBD plane and selecting the closest pad with an amplitude greater than 4σ of the pedestal distribution. An example of matching distributions for hadrons and electrons in FB and RB configurations are shown in fig. 3 and fig. 4.

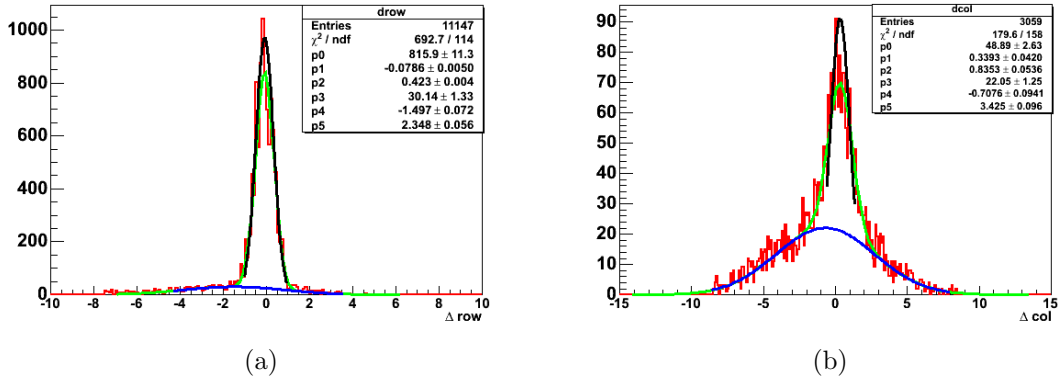


Figure 3: Matching distributions for hadrons in FB(left) and RB(right). The underlying background of random matches is shown by green line.

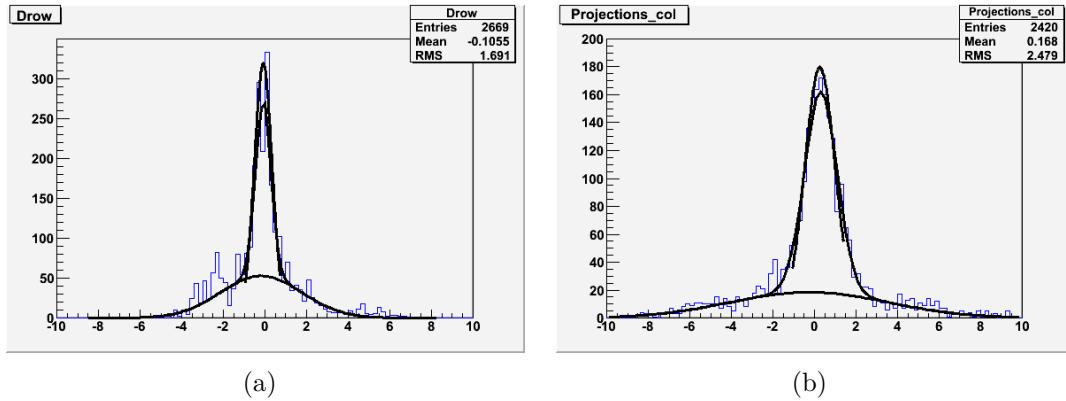


Figure 4: Matching distributions for electrons in FB(left) and RB(right). The underlying background is shown by the green line.

Adjacent pads with an amplitude $> 4\sigma$ of the pedestals are associated with the closest pad to define the hit cluster. The Čerenkov blob size produced by a single electron in the HBD is shared by 2-3 pads on the average. To allow for complete cluster reconstruction, tracks are rejected if the closest HBD hit is at the edge of the detector. Hadrons, on the other hand mostly produce a single pad cluster.

The prototype results demonstrated the basic properties of the HBD i.e. hadron blindness and electron hadron separation. Fig. 5 shows the charge distribution for minimum ionizing particles obtained in the FB(blue) and RB(red) configurations.

The two figures correspond to a detector gain of 2200 (left panel) and 6600 (right panel). As can be seen, the FB spectrum is nicely fitted with a Landau distribution, a prominent feature of the energy loss of a minimum ionizing particle (mip). The RB spectrum on the other hand clearly shows a strong suppression of the direct ionization signal, as expected.

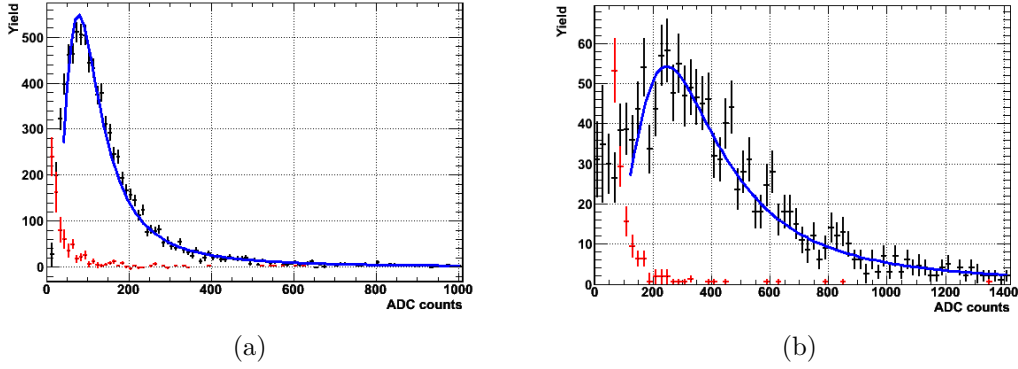


Figure 5: Pulse height distribution for minimum ionizing particles for detector gain 2200 (a) and 6600 (b) respectively. Black represents FB and red represents RB.

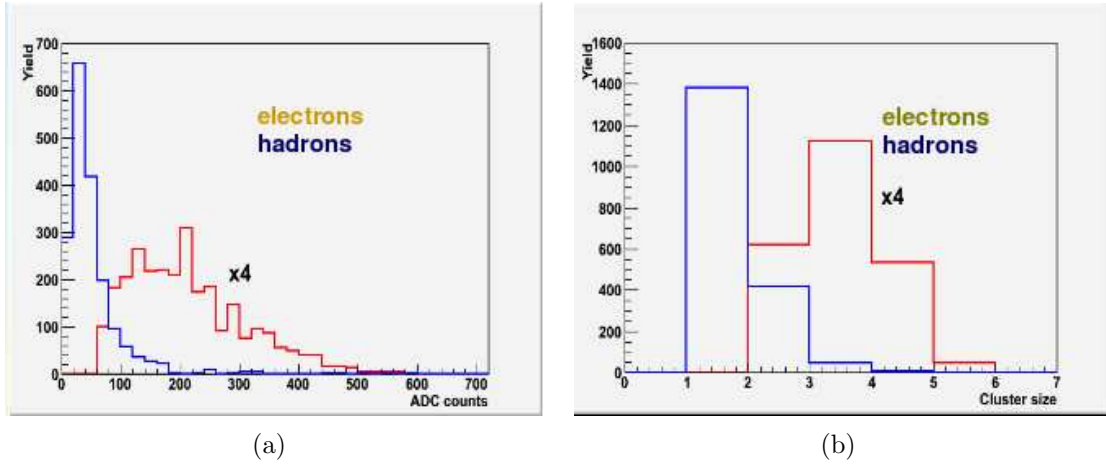


Figure 6: Charge distribution (a) and cluster size distribution (b) for identified electrons and hadrons with the HBD prototype operated in reverse bias mode.

A clear distinction of the HBD response to electrons and hadrons can be seen in Fig. 6. The left plot is the charge distribution and the right one is the cluster size distribution for electrons and hadrons in the RB scenario. A cut on the pulse height alone gives a rejection factor of 15 with an electron efficiency of 90%. A further enhancement in the rejection factor can be achieved by combining the pulse height and cluster size information.

4 Construction of the final HBD for PHENIX

The design and construction of the detector vessel as well as assembly and preliminary test of the GEM foils were carried out at the WIS whereas *CsI* evaporation, final assembly and test of detector modules were done at the Stony Brook University. The analog and digital electronics were developed and built by BNL Instrumentation and Columbia University.

4.1 Vessel construction

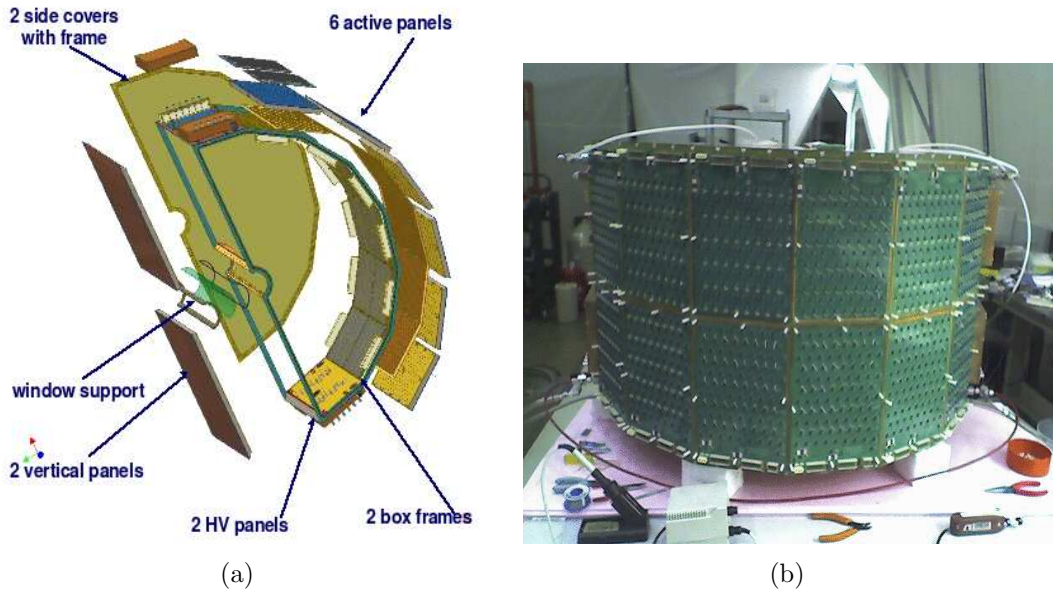


Figure 7: The left panel shows a 3-d view of the HBD final design and the right panel shows almost completed one half of the HBD vessel with the pre-amps installed on the back side.

The HBD consists of two identical vessels. An exploded view of one vessel with one side panel removed for clarity can be seen in Fig. 7(a). Each vessel has a polygonal shape and is made up of 10 panels glued together. Two FR4 frames 7 mm thick, provide mechanical stability and rigidity to the structure. The two side covers are attached to the vessel frames with plastic screws and an O-ring seal. The panels are made up of 19 mm thick honeycomb core, glued on each side to a 0.25 mm thick FR4 sheet. The side covers have a similar structure but use a 13 mm thick honeycomb core. The entrance window to the detector is a 127 μm thick mylar foil coated with 100 nm aluminum and is placed between two FR4 supports bolted to each other with an O-ring seal.

Each of the six active back panels is equipped with two triple GEM photon detectors on the inside and to the Front End Electronics on the outer side. The two panels outside the active area are used for detector services such as gas in/out, high voltage boxes and UV transparent windows. The detector anode is a double-sided printed circuit board (PCB) made of a 50 μm thick Kapton foil in one single piece

($140 \times 63 \text{ cm}^2$) and has 1152 hexagonal pads on the inner side and short (1.5 cm long) signal traces on the outer side, connected to the pads by plated through holes in the PCB. Making the PCB as a single piece and gluing it to the panels provide a good seal at the junctions between the panels. The various operations like gluing, assembling the panels etc were done with specially designed jigs and tools. The vessel construction involved ~ 350 gluing operations per box.

Special care was taken in the design to minimize the dead areas, multiple scattering and conversions within the central arm acceptance. Each box weighs ~ 5 Kg. Adding all accessories, HV connectors, gas in/out, GEM foils, preamplifier cards etc, results in a total weight of less than 10 Kg. The HBD contributes a total radiation length of about 3.14%, inside the central arm acceptance out of which 0.919% comes from vessel, 1.88% from the electronics installed on the back of vessel and 0.54% from the 50 cm long CF_4 radiator.

It is extremely important to have a leak-tight detector. Both the water and oxygen have absorption bands in the deep UV region that absorb Čerenkov light and reduce the overall photoelectron yield. Every 10 ppm of either oxygen or water result in a loss of approximately 1 photoelectron due to absorption in a 50 cm long CF_4 radiator. The water also adversely affects the photocathode performance, reducing its quantum efficiency. The leak-rate in each one of the 311 litres vessel was measured to be $< 0.12 \text{ cc/min}$.

4.2 Assembly and Testing of GEM foils

The HBD consists of 24 identical detector modules, 12 in each arm, 6 along $\varphi \times 2$ along z with a size $23 \times 27 \text{ cm}^2$. Each detector module is comprised of a 90% transparent stainless steel mesh and three GEM detectors. A standard GEM foil is a thin ($50 \mu\text{m}$) Cu-clad ($5 \mu\text{m}$) kapton foil perforated with holes of $80 \mu\text{m}$ diameter at a pitch of $150 \mu\text{m}$. The top GEM facing the detector volume has a 0.2-0.4 μm layer of CsI evaporated on its surface previously coated with thin Gold and Nickel layers. The Gold layer prevents chemical reaction of the CsI with the copper of the GEM and the Ni acts as an adhesive agent between gold and copper. One surface of the GEM foil is divided into 28 HV segments to reduce the capacitance and stored energy in case of discharge. The entrance mesh and the three GEM foils are mounted on FR4 fiberglass frames. The frames have a width of 5 mm and a thickness of 1.5 mm that defines the inter-gap distance. They also have a supporting cross shape (0.3 mm thick in the middle), which prevents sagitta of the foils in the electrostatic field. The three GEM foils and mesh are stacked together and attached to the detector vessel by 8 pins, located at the corners and middle of the frames, that maintain the tension and prevent deformation of the 5 mm wide frames. The design allowed for only 1 mm clearance between two adjacent detectors. With this design, the resulting total dead area within the central arm acceptance is calculated to be 6%.

The different operations like gluing, stretching and high voltage testing of the GEM foils was done either in a clean room or in a stainless steel box. The GEM foil was first stretched on a special stretching device and while stretched, glued onto the FR4 frames using epoxy. Once the epoxy was cured, the GEM foil was cut from

the stretching device and SMD resistors were soldered across each HV segment. The GEMs were monitored for leakage current and discharges at every step namely before framing, after gluing and after soldering the resistors. A good GEM was required to draw current below 5 nA. A GEM that passed all these quality control tests was then mounted inside a stainless steel vessel and was tested up to 520V in CF₄. It was then mapped for gain variations in Ar/CO₂ using a collimated ⁵⁵Fe source, positioned inside the box. The measured gain values (corrected for pressure and temperature variation) were then stored in the PHENIX database.

Due to small differences in the hole diameters, the GEMs have local gain variations that lead to an additive effect in the triple GEM assembly. A random combination of GEMs for the triple GEM assembly thus led to local gain variations which could be as high as 50%. In order to have the lowest possible gain variations in all modules, gain maps of the single GEMs were used to determine all possible triplets combinations and the best ones leading to the smallest gain variations were selected. The resulting gain spread for module to module varied from 5% to 20% in all the 24 modules. Fig. 8 shows the measured gain uniformity of an installed stack in the HBD selected using this strategy. Out of a total of 65 standard and 47 gold plated GEMs that passed all the quality assurance tests, 48 standard and 24 Gold GEMs were used to construct the final detector.

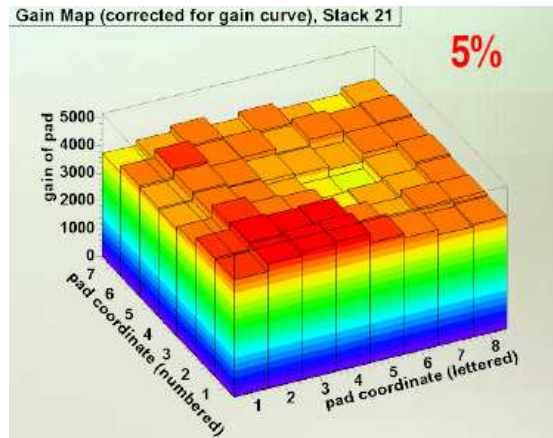


Figure 8: Gain map of one of the triple GEM stacks presently installed in the HBD

4.3 Readout electronics

Circuit boards containing the readout electronics were installed on the back side of the vessel. The readout board is a multilayer board which contains the preamps and has a signal layer that drives the differential output signals from the preamps to connectors located at the edge of the board. The preamps used are hybrid preamplifiers, the *IO1195 - 1*, developed by the Instrumentation Division at BNL. The gain is set to give an output signal of ± 50 mV for an input signal of 16fC (100,000 e's), corresponding to an average signal of 20 photoelectrons per pad at a gas gain of 5×10^3 . The preamp signals are digitized using a flash ADC.

5 Present status and Future Plans

5.1 HBD Commissioning

The construction of the HBD has been completed recently. Both vessels have been fully instrumented and are installed in the PHENIX set-up. The HBD is currently undergoing all commissioning tests and is in data taking mode for the ongoing Au - Au run. Relative CsI quantum efficiency measurements are done at regular intervals to monitor the stability of the CsI photocathodes. A high purity recirculation gas system is used to flow CF_4 through the detector. The level of O_2 and H_2O are monitored at the input and output of the vessels. Additionally, a monochromator is used for monitoring the UV transmission for the input and output gas.

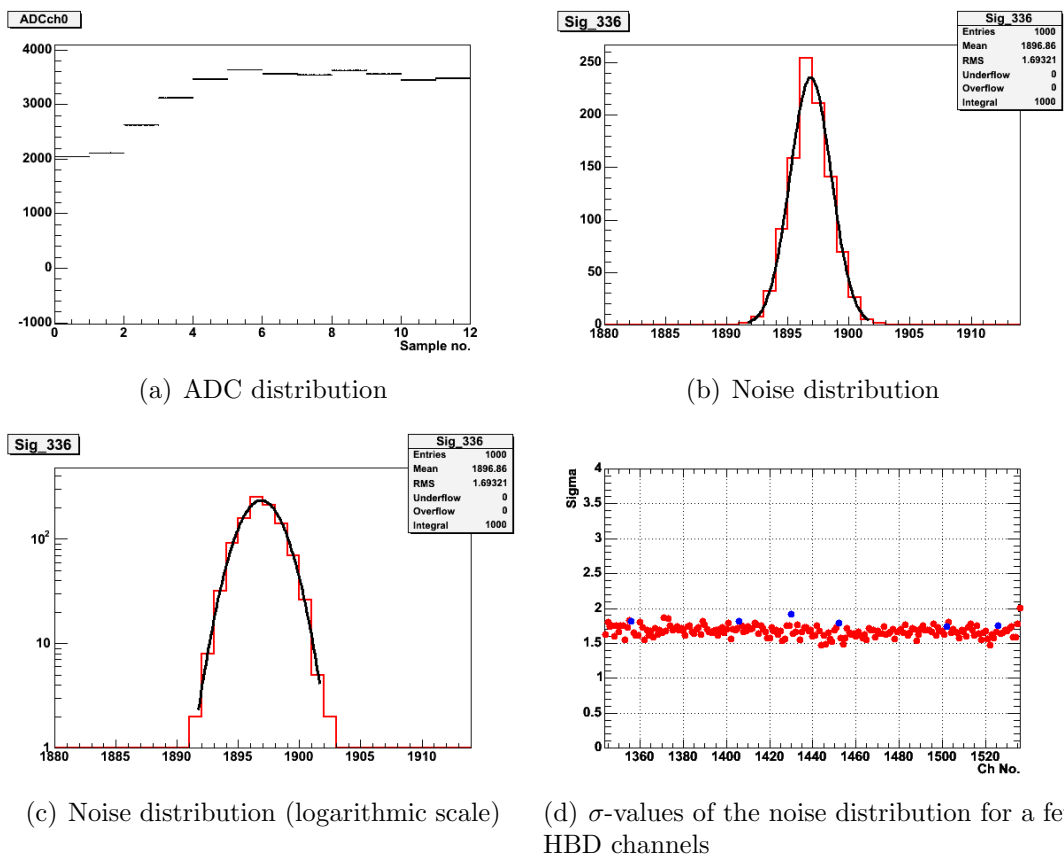


Figure 9: ADC and Noise distributions for the final HBD

The readout chain is fully operational and checked. The amplified differential signals produced by pre-amps are delivered to a receiver and front end module (FEM). The FEM contains a 12 bit, 65 MHz flash-ADC for each channel and samples the signal 6 times per RHIC beam crossing at $\sim 6 \times 9.4$ MHz. An example of a 12×16 ns sample TDC signal for one HBD pad can be seen in fig. 9(a). The best algorithm for signal processing is $(S[8] + S[9] + S[10])/3 - S[0]$. One can see fig. 9(b) (linear scale) and fig. 9(c) (logarithmic scale), the baseline noise distributions, very nicely fitted with a gaussian. The noise level (as can be seen in fig. 9(b) and 9(d)), is typically $\sigma \sim 1.5$ ADC counts corresponding to ~ 0.37 primary electrons at a gain of 10^4 . A zero suppression algorithm has been being implemented that helps reducing

the event size.

The high voltage and the related software for the HBD is fully operational. The HV to the HBD is provided by means of LeCroy 1458 mainframes and LeCroy high voltage modules [15]. Each detector module uses two power supplies, i.e. a total of 48 power supplies for the whole HBD. A three branch resistive chain circuit with one single HV power supply is used to power the three GEMs while the second power supply is used for the mesh. The main advantage of three branch resistive chain is that if a short occurs in one of the HV segments of one GEM, the two other GEMs will be totally unaffected.

A Graphical User Interface is used to bring the HBD modules, individually or as a group, to the desired voltage, enable and disable them, auto-recover the trips etc. The software has also been incorporated with the additional capability of inserting into the PHENIX database all the information related to the modules like measured current, voltage and all other useful parameters, whenever there is some change in the module state. This information is then processed by additional scripts and serves as an efficient way to monitor the detector stability and conditioning processes.

5.2 Plans

At present, I am involved in the data taking with the HBD in the ongoing run, looking into the initial gain measurements and monitoring the detector status. I will analyze the data being collected to assess the detector performance using the analysis method that I developed for the full scale prototype studies. I am also working on the Monte Carlo simulations for the HBD to study the system performance by estimating signal efficiency in HBD and the expected improvement of the S/B ratio. For this a few million of Hijing Au-Au events were generated and passed through the PHENIX simulation software (PISA). The next steps involve embedding these events with $\phi \rightarrow e^+e^-$ and passing through PHENIX reconstruction and tracking.

6 Run 5 pp analysis

I am analyzing the production of low-mass e^+e^- pairs in pp collisions using the run 5 data. High energy pp collisions provide the necessary baseline in the understanding of pA and AA collisions. During the year 2005, RHIC provided proton - proton collisions at $\sqrt{s_{NN}} = 200$ GeV. In order to benefit from the high luminosity in pp collisions and to efficiently detect electrons, PHENIX uses an electron trigger (ERT). This trigger combines the information from two central arm detectors: the Electromagnetic Calorimeter(EMCal) and the Ring Imaging Čerenkov detector (RICH). It requires an event to have at least one track with an energy above a certain threshold in EMCal and then a geometrical correlation between the RICH and EMCal completes the electron identification. During run 5, PHENIX collected 1.65B ERT events.

Events and track selection

The analysis is restricted to events with the collision vertex between $-30 \leq z_{BBC} \leq$

28 cm as defined by the Beam Beam Counters of PHENIX. The charged particle momentum and trajectory are defined by the Drift Chamber(DC) and Pad Chamber(PC1). The reconstructed tracks are further confirmed by the matching between the projected and associated hits information at the EMCal and RICH.

Electron identification in PHENIX is provided by the RICH and EMCal detectors. A track is identified as electron if it fires at least one photo-multiplier tube (PMT) in the RICH associated to it. However, hadrons can be misidentified as electrons by a random association with an unrelated hit in the RICH. The hadron background is thus removed by comparing the track momentum, measured by the DC to the energy deposited in the EMCal. For electrons, the E/p is required to be greater than 0.5.

Matching to EMCal

The track matching to the EMCal along the z and φ - co-ordinates as well as E/p distributions are momentum and particle charge dependent. An example of raw distributions for these three variables for electrons for one EMCal sector E0 and p_t bin 0.05 - 0.35 GeV/c, can be seen in the fig. 10.

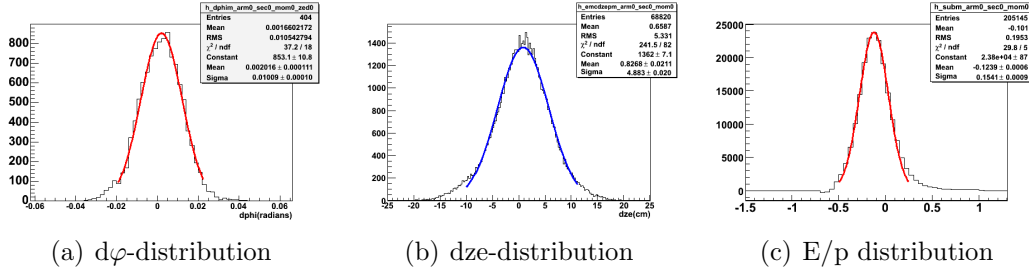


Figure 10: Track matching along the z - and φ - co-ordinates and E/p distribution for sector E0 and momentum bin 0.05 - 0.35 GeV/c, fitted with gaussian function.

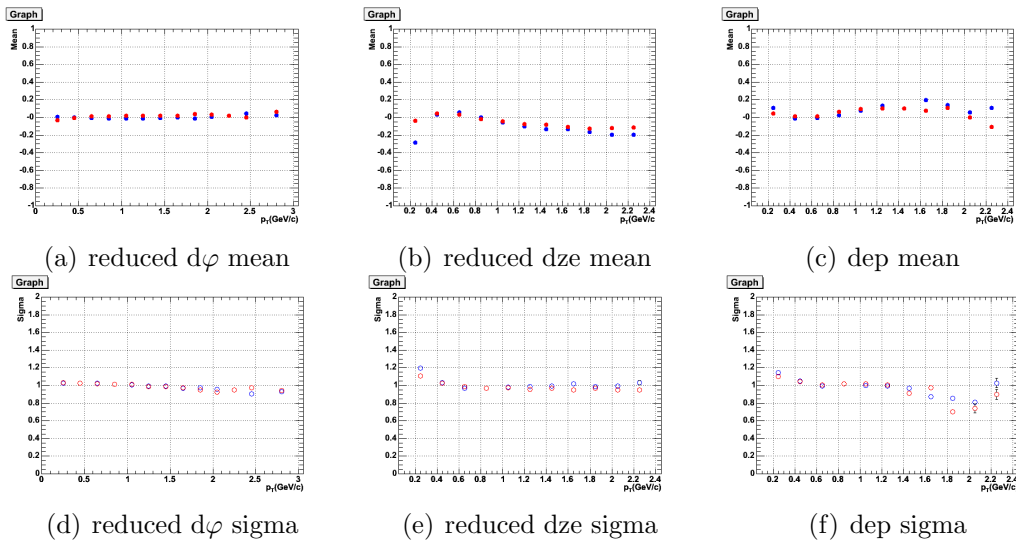


Figure 11: Mean and Sigma of track matching along z - and φ - co-ordinates and $E/p-1$ distributions as a function of p_T for one EMCal sector for the east arm

For the analysis, the E/p values and the spatial matching in the z - and φ -directions are translated into reduced variables. The raw distributions of the track matching and E/p-1 are fitted with a Gaussian function for each EMCAL sector and momentum bin, separately for electrons and positrons selected by applying strong RICH cuts. The φ -distribution for each momentum bin in addition was segmented into z -vertex bins and then fitted to remove the residual magnetic field dependence. The reduced variables are calculated using the mean and sigma derived from the fit as shown in eq. (1).

$$X^{Reduced} = \frac{X - (Mean_of_the_fit)}{(Sigma_of_the_fit)} \quad (1)$$

The distributions are then centered at zero and have sigmas equal to one. An example of reduced mean values and sigmas as a function of p_T , obtained by using the above procedure for the three variables, is shown in fig. 11 for one EMCAL sector in the east arm. The reduced variables are convenient for applying cuts in the units of sigmas.

Optimization of Cuts and Mass spectrum

The e^+e^- invariant mass spectrum is derived by combining all the identified electrons to form pairs. The electrons are identified by applying the standard eID cuts used in PHENIX. In addition, a few pair cuts are used that take care of rejecting the artificial tracks and conversions that are produced by beam pipe. The cut values used in the analysis are optimized by studying their effect on the ϕ -meson yield derived from the data and using simulations. The resulting e^+e^- unlike invariant mass spectrum thus obtained is shown in the fig. 12.

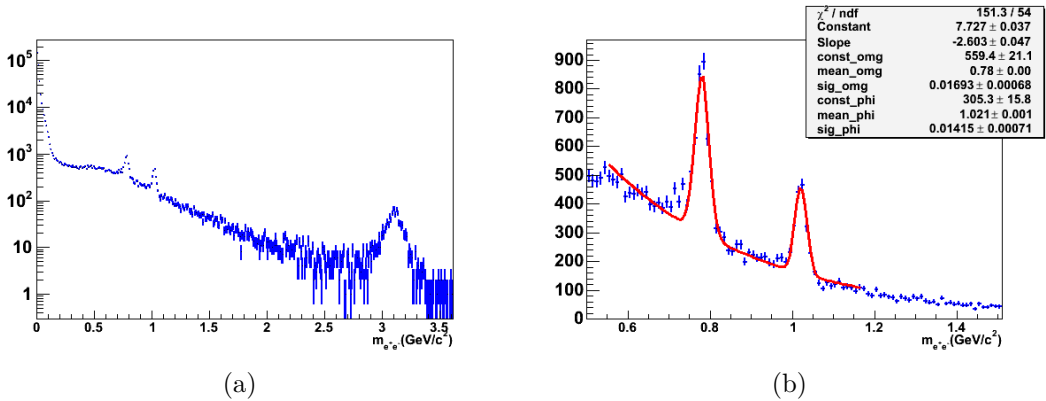


Figure 12: The left panel shows the full invariant e^+e^- mass spectrum and the right panel shows the zoomed spectra in ϕ and ω mass region.

Plans

The plan is to finish the analysis of pp data in run5. This involves extracting the absolute yield and shape of the low-mass continuum as well as the vector meson resonances ω and ϕ . This also includes the Monte Carlo simulations to take into

account the acceptance, reconstruction and embedding effects. Trigger efficiency calculations and run by run efficiency also needs to be done.

References

- [1] F. Karsch, Lect. Notes Phys. 583, (2002) 209, hep-lat/0106019.
- [2] G. Agakichiev, et al. (CERES Collaboration), Phys. Rev. Lett. 75(1995)1272.
- [3] D. Adamova et al. Phys. Rev. Lett. 91 (2003)042301. [arXiv: nucl-ex 10209024]
- [4] R. Rapp and J. Wambach, Adv.Nucl.Phys.25(2000)[arXiv:hep-ph/9909229].
- [5] G. E. brown and M. Rho, Phys.Rept.363(2002) 85[arXiv:hep-ph/0103102].
- [6] R. Rapp, nucl-th/0204003(2002).
- [7] PHENIX detector overview K.Adcox et al., NIM A499 469-477(2003).
- [8] Technical Note 391: Proposal for a Hadron Blind Detector for PHENIX, 2001.
- [9] F. Sauli, Nucl. Instr. and Meth. A523 (2004), 345
- [10] A. Kozlov, I. Ravinovich, L. I. Shekhtman, Z. Fraenkal, M. Inzuka and I. Tserruya, Nucl. Instrum. Meth A523, 345(2004)[arXiv: physics/0309013].
- [11] Z. Fraenkel et al., Nucl. Instrum. Meth. A546, 466(2005) [arXiv: physics/0502008].
- [12] A. Milov eta al., arXiv: physics/0701273
- [13] I.Tserruya et.al.,”A Hadron Blind Detector for the PHENIX Experiment at RHIC”, Conference Record Proceedings of the 2004 IEEE Nuclear Science Symposium and Medical Imaging Conference, Oct 16-22, 2004, Rome, Italy.
- [14] J. A. Kamin, Eur. Phys. J. C49, 177-180(2007).
- [15] http://www.phenix.bnl.gov/phones/oncs/Anc_sys/hvmanual.ps.
- [16] S.S. Adler et al. (PHENIX collaboration) PPG 16, to be published in Phys. Rev, C.